

# Instantaneous Real-time Cycle-slip Correction for Quality Control of GPS Carrier-Phase Measurements

Donghyun Kim and Richard B. Langley

*Geodetic Research Laboratory, Department of Geodesy and Geomatics Engineering,  
University of New Brunswick, Fredericton, N.B., Canada E3B 5A3*

**ABSTRACT:** *This paper proposes a new cycle-slip correction method which enables instantaneous correction (i.e., using only current epoch's GPS carrier-phase measurements) at the data quality control stage. The method was originally developed for real-time applications which require consistent high-precision positioning results with the carrier-phase measurements at 10 Hz data rate. The approach includes: 1) two parameters for generating and filtering cycle-slip candidates; and 2) a validation procedure which authenticates correct cycle slip candidates. Compared with conventional approaches utilizing carrier phases and pseudoranges, the approach does not require a smoothing or filtering process to reduce observation noise. Therefore, it is possible to implement the approach in real-time applications without undue complexity. Additionally, the approach enables the determination of system performance (e.g., integrity and continuity) by assigning the confidence level of the parameters for cycle-slip candidates in designing the system. Simulation tests were conducted to confirm the performance of the approach under the worst case scenarios. Test results carried out in a variety of situations including static and kinematic modes, short-baseline and long-baseline situations, and low and high data rates are presented.*

## INTRODUCTION

In order to attain consistent high-precision positioning results with GPS carrier-phase measurements, errors unspecified in a functional or stochastic model (errors of omission) must be correctly detected and removed or otherwise handled at the data processing stage. Such errors in the carrier-phase measurements may include cycle slips, receiver clock jumps, multipath, diffraction, ionospheric scintillation, *etc.* Reliability, which refers to the ability to detect such errors and to estimate the effects that they may have on a solution, is one of the main issues in quality control. Texts containing detailed discussions of this topic include those by Leick [1] and Teunissen and Kleusberg [2]. A comprehensive investigation of quality issues in real-time GPS positioning has been carried out by the Special Study Group (SSG) 1.154 of the International Association of Geodesy (IAG) during 1996-1999 [3].

The effects of cycle slips and receiver clock jumps can be easily captured either in the measurement or parameter domain due to their systematic characteristics. Their systematic effects on the carrier-phase measurements can be almost completely removed once they are correctly detected and identified. On the other hand, multipath, diffraction, ionospheric scintillation, *etc.* have temporal and spatial characteristics which are more or less quasi-random. These quasi-random errors cannot be completely eliminated and must be handled using a rigorous mathematical approach such as data snooping theory [4]. However, statistical testing and reliability analysis can only be efficient if the stochastic models are correctly known or well approximated. As has been experienced, quasi-random errors are often mixed with systematic ones in real world situations. One reasonable approach for handling errors in such situations is to separate the systematic ones from the quasi-random ones. Estimating the quasi-random errors after removing the systematic ones can provide more reliable results in terms of least-squares estimation. This is the main idea implemented in our quality control algorithm including cycle-slip correction as depicted in Figure 1.

This paper addresses the development of a cycle-slip correction technique designed to detect and correct cycle slips in dual-frequency, carrier-phase data in a real-time environment as a part of a quality control algorithm. Our approach was originally developed for real-time GPS kinematic applications requiring sub-centimetre accuracy with high-rate data (*e.g.*, 10 Hz). For the completeness of our discussions, we will first look at the characteristics of the errors of interest. Then, a brief explanation of our approach for cycle-slip correction will be given. Several difficult situations, which can be considered as the worst cases in real world situations, will be discussed to answer the crucial question: "How perfectly can the method work?" Test results will be presented and discussed, followed by conclusions.

## ANOMALOUS OBSERVATION DATA

The quality of GPS positioning is dependent on a number of factors. To attain high-precision positioning results, we need to identify the main error sources impacting on the quality of the measurements. In terms of data processing, receiver clock jumps, cycle slips and quasi-random errors are the main sources which can deteriorate the quality of the measurements and subsequently, the quality of positioning results.

### *Receiver Clock Jumps*

Most receivers attempt to keep their internal clocks synchronized to GPS Time. This is done by periodically adjusting the clock by inserting time jumps. The actual mechanism of how the clock in a particular manufacturer's receiver is adjusted is typically proprietary. However, like cycle slips, their effects on the code and phase observables are more or less known to users and hence it is possible to remove their effects almost completely. At the moment of the clock correction, two main effects are transferred into the code and phase observables as illustrated in the following equation:

$$\Psi(t+\Delta) \approx \Psi(t) + \dot{\Psi} \cdot \Delta \approx \Psi(t) + \dot{\rho} \cdot \Delta - c \cdot \Delta, \quad (1)$$

where  $\Psi$  represents the carrier-phase (or pseudorange) measurements (in distance units) and  $\dot{\Psi}$  its time rate of change;  $\Delta$  is the clock jump (in time units) which is assumed to be a very small value (*e.g.*, less than or equal to one millisecond);  $\dot{\rho}$  is the geometric satellite-receiver range rate (in distance per time units); and  $c$  is the vacuum speed of light. The effects of the geometric range corresponding to the clock jump ( $c \cdot \Delta$ ) are common to all measurements at the moment of the clock jump at one receiver. By single-differencing (SD) the measurements between satellites or double-differencing (DD) the measurements (that is, differencing between receivers followed by differencing between satellites or vice versa), the common effects can be removed. However, the effects of the geometric range rate corresponding to the jump ( $\dot{\rho} \cdot \Delta$ ) are different for each observation. They cannot be removed by the SD operation. Instead, Doppler frequency or carrier-phase difference measurements should be used for correcting such effects. The clock jumps can be easily detected in both the measurement and parameter domains.

### *Cycle Slips*

Cycle slips are discontinuities of an integer number of cycles in the measured (integrated) carrier phase resulting from a temporary loss-of-lock in the carrier tracking loop of a GPS receiver. In this event, the integer counter is re-initialized which causes a jump in the instantaneous accumulated phase by an integer number of cycles. Three causes of cycle slips can be distinguished [5]: First, cycle slips are caused by obstructions of the satellite signal due to trees, buildings, bridges, mountains, *etc.* The second cause of cycle slips is a low signal-to-noise ratio (SNR) or alternatively carrier-to-noise-power-density ratio ( $C/N_0$ ) due to severe ionospheric conditions, multipath, high receiver dynamics, or low satellite elevation angle. A third cause is a failure in the receiver software which leads to incorrect signal processing.

Cycle slips in the phase data must be corrected to utilize the full measurement strength of the phase observable. The process of cycle-slip correction involves detecting the slip, estimating the exact number of L1 and L2 frequency cycles that comprise the slip, and actually correcting the phase measurements by these integer estimates. Cycle slip detection and correction requires the location of the jump and the determination of its size. It can be completely removed once it is correctly detected and identified.

### *Quasi-random Errors*

Multipath, diffraction, ionospheric scintillation, *etc.* may be the main sources of quasi-random errors, which are apt to be omitted in the functional and stochastic models. Since least-squares estimation, when errors are present, tends to hide (reduce) their impact and distribute their effects throughout the entire set of measurements, it is better to handle cycle slips and clock jumps separately from quasi-random errors. To detect and remove quasi-random errors, we have to test a null hypothesis (that is, no errors in the measurements) against an alternative hypothesis which describes the type of mis-specifications in the models (see [1] and [2]).

## AN INSTANTANEOUS CYCLE-SLIP CORRECTION TECHNIQUE

One of the various methods for detecting and identifying cycle slips is to obtain the triple-difference (TD) measurements of carrier phases first. By triple-differencing the measurements (that is, at two adjacent data collection epochs, differencing

the DD measurements) biases such as the clock offsets of the receivers and GPS satellites, and ambiguities can be removed. The TD observables (in distance per time units) are

$$\begin{aligned}\delta\nabla\Delta\Phi_1 &= \delta\nabla\Delta\rho + \lambda_1 \cdot \nabla\Delta C_1 + \delta\nabla\Delta s + \delta\nabla\Delta\tau - \delta\nabla\Delta I + \delta\nabla\Delta b_1 + \delta\nabla\Delta\varepsilon_1 \\ \delta\nabla\Delta\Phi_2 &= \delta\nabla\Delta\rho + \lambda_2 \cdot \nabla\Delta C_2 + \delta\nabla\Delta s + \delta\nabla\Delta\tau - \gamma \cdot \delta\nabla\Delta I + \delta\nabla\Delta b_2 + \delta\nabla\Delta\varepsilon_2,\end{aligned}\quad (2)$$

where  $\Phi$  is the measured carrier phase;  $\rho$  is the geometric range from receiver to GPS satellite;  $\lambda$  is the carrier wavelength;  $C$  is a potential cycle slip (in cycle units);  $s$  is the satellite orbit bias;  $\tau$  is the delay due to the troposphere;  $I$  is the delay of L1 carrier phase due to the ionosphere;  $\gamma = (\lambda_2 / \lambda_1)^2 \approx 1.65$ ;  $b$  is multipath;  $\varepsilon$  is receiver system noise; subscripts “1” and “2” represent L1 and L2 carrier phases, respectively; and  $\nabla\Delta$  and  $\delta\nabla\Delta$  are the DD and TD operators, respectively. Satellite and receiver instrumentation biases, assumed constant, are ignored.

In most GPS applications, regardless of surveying mode (static or kinematic) and baseline length (short, medium or long), the effects of the triple-differenced biases and noise (*i.e.*, atmospheric delay, satellite orbit bias, multipath, and receiver system noise) are more or less below a few centimetres in size as long as the observation sampling interval is relatively short (*e.g.*, sampling interval less than 1 minute). There could be exceptional situations such as an ionospheric disturbance, extremely long baselines, and huge (rapid) variation of the heights of surveying points in which the combined effects of the biases and noise can exceed the wavelengths of the L1 and L2 carrier phases. However, to simplify our discussion, we will assume, for the time being, that such situations can be easily controlled through adjusting the sampling rate so that the combined effects of the biases and noise can be reduced to a level below a few centimetres. In the section “Cycle-Slip Candidates”, we will see that we can remove this assumption.

### **Cycle-Slip Observables**

As revealed in equation (2), the geometric range should be removed to estimate the size of cycle slips. If we can replace the TD geometric ranges with their estimates, then the TD carrier-phase prediction residuals become

$$\begin{aligned}\delta\Phi_{TD1} &= \delta\nabla\Delta\Phi_1 - \delta\nabla\Delta\hat{\rho} = \lambda_1 \cdot \nabla\Delta C_1 + \varepsilon'_1 \\ \delta\Phi_{TD2} &= \delta\nabla\Delta\Phi_2 - \delta\nabla\Delta\hat{\rho} = \lambda_2 \cdot \nabla\Delta C_2 + \varepsilon'_2,\end{aligned}\quad (3)$$

where

$$\begin{aligned}\varepsilon'_1 &= \delta\rho_{TD} + \delta\nabla\Delta s + \delta\nabla\Delta\tau - \delta\nabla\Delta I + \delta\nabla\Delta b_1 + \delta\nabla\Delta\varepsilon_1 \\ \varepsilon'_2 &= \delta\rho_{TD} + \delta\nabla\Delta s + \delta\nabla\Delta\tau - \gamma \cdot \delta\nabla\Delta I + \delta\nabla\Delta b_2 + \delta\nabla\Delta\varepsilon_2,\end{aligned}\quad (4)$$

and  $\delta\rho_{TD} (= \delta\nabla\Delta\rho - \delta\nabla\Delta\hat{\rho})$  represents the prediction residuals of the TD geometric ranges. Therefore, the TD carrier-phase prediction residuals will be a good measure for detecting and correcting cycle slips if the effects of the residuals in equation (4) are small.

### **TD Geometric Range Estimation**

To obtain the estimates of the TD geometric ranges, we need another observable which is immune from cycle slips. The Doppler frequency and the TD pseudoranges can be used for this purpose. The former is preferable to reduce the effects of the residuals in equation (4). Using the Doppler frequency at two adjacent data collection epochs, we have

$$\delta\nabla\Delta\hat{\rho}_k = -(\nabla\Delta D_k + \nabla\Delta D_{k-1})/2, \quad (5)$$

where  $D$  is the Doppler frequency (in distance per time units); subscripts “ $k$ ” and “ $k-1$ ” represent the time tags of two adjacent data collection epochs and the sign is reversed due to the definition of Doppler shift. For some receivers from which the Doppler frequency is not available to users, the TD pseudoranges (a noisier observable than the Doppler frequency) can be used instead. In this case, the estimate of the TD geometric range is given as:

$$\delta\nabla\Delta\hat{\rho}_k = (\delta\nabla\Delta P_k - \delta\nabla\Delta P_{k-1})/\delta t, \quad (6)$$

where  $P$  is the measured pseudorange and  $\delta t (= t_k - t_{k-1})$  is the time interval between two adjacent data collection epochs.

### Cycle-Slip Candidates

Consider the first two moments of the TD carrier-phase prediction residuals

$$\begin{aligned} E[\delta\Phi_{TDi}] &= \lambda_i \cdot \nabla \Delta C_i, \quad i=1,2 \\ Cov[\delta\Phi_{TDi}] &= Cov[\varepsilon'_i], \end{aligned} \quad (7)$$

where  $E[\cdot]$  and  $Cov[\cdot]$  are the mathematical expectation and variance-covariance operators. Since there is no redundancy to carry out statistical testing for equations (7), we will use it to obtain the cycle-slip candidates. In this case, we need *a priori* information for the second moment. This can be obtained either through system tuning or adaptive estimation. This means that we do not have to assume specific models for the biases and noise in equation (4). Introducing a threshold associated with the second moment, we can obtain the cycle-slip candidates as:

$$\begin{aligned} |\lambda_i \cdot CS_i - \delta\Phi_{TDi}| &\leq \varepsilon_{CS_i}, \quad i=1,2 \\ \varepsilon_{CS_i} &= k \cdot \sqrt{Cov[\varepsilon'_i]}, \end{aligned} \quad (8)$$

where  $CS_i (\in \mathbb{Z})$  represents the cycle-slip candidates;  $\varepsilon_{CS_i}$  is a threshold value derived from the second moment; and  $k$  is a scale factor which can define the level of integrity in designing the quality control routine.

### Filtering of Cycle-Slip Candidates

When dual-frequency carrier phases are available, we can reduce, to a large extent, the number of cycle-slip candidates using the TD geometry-free phase (a scaled version of which is called the differential ionospheric delay rate). The TD geometry-free phase (in distance per time units) is

$$\begin{aligned} \delta\Phi_{GF} &= \delta\nabla\Delta\Phi_1 - \delta\nabla\Delta\Phi_2 \\ &= (\lambda_1 \cdot \nabla\Delta C_1 - \lambda_2 \cdot \nabla\Delta C_2) + \varepsilon'', \end{aligned} \quad (9)$$

where

$$\varepsilon'' = (\gamma - 1)\delta\nabla\Delta I + (\delta\nabla\Delta b_1 - \delta\nabla\Delta b_2) + (\delta\nabla\Delta\varepsilon_1 - \delta\nabla\Delta\varepsilon_2). \quad (10)$$

Compared with equation (4), the effects of the residuals in equation (10) are usually smaller. We can also consider the first two moments of the TD geometry-free phase

$$\begin{aligned} E[\delta\Phi_{GF}] &= \lambda_1 \cdot \nabla\Delta C_1 - \lambda_2 \cdot \nabla\Delta C_2 \\ Cov[\delta\Phi_{GF}] &= Cov[\varepsilon'']. \end{aligned} \quad (11)$$

In conjunction with equations (8), equations (11) can be used to filter out most cycle-slip candidates which are not real cycle slips. A threshold test is given as:

$$\begin{aligned} |CS' - \delta\Phi_{GF}| &\leq \varepsilon_{GF} \\ \varepsilon_{GF} &= k \cdot \sqrt{Cov[\varepsilon'']}, \end{aligned} \quad (12)$$

where  $CS' = \lambda_1 \cdot CS_1 - \lambda_2 \cdot CS_2$ ;  $\varepsilon_{GF}$  is a threshold value derived from the second moment; and  $k$  is the scale factor used in equations (8). An exceptional case is the combination-insensitive cycle-slip pairings of which the expectation in equations (11) is close to zero. We will discuss this case in the section ‘‘Worst Case Simulation Scenarios’’.

### Cycle-Slip Validation

Fixing cycle slips in the TD measurements is conceptually the same problem as resolving ambiguities in the DD measurements. Consider the linearized model of the TD observables in equations (2):

$$\begin{aligned} \mathbf{y} &= \mathbf{A}\mathbf{c} + \mathbf{B}\mathbf{x} + \mathbf{e}, \quad \mathbf{c} \in \mathbb{Z}^n, \quad \mathbf{x} \in \mathbb{R}^u \\ \text{Cov}[\mathbf{y}] &= \mathbf{Q}, \end{aligned} \quad (13)$$

where  $\mathbf{y}$  is the  $n \times 1$  vector of the differences between the TD measurements and their computed values;  $n$  is the number of measurements;  $\mathbf{c}$  is the  $n \times 1$  vector of the cycle-slip candidates;  $\mathbf{x}$  is the  $u \times 1$  vector of all other unknown parameters including position and other parameters of interest;  $u$  is the number of all other unknowns except cycle slips;  $\mathbf{A}$  and  $\mathbf{B}$  are the design matrices of the cycle-slip candidates and the other unknown parameters;  $\mathbf{e}$  is the  $n \times 1$  vector of the random errors. The first step for cycle-slip validation is to search for the best and second best cycle-slip candidates which minimize the quadratic form of the residuals. The residuals of least-squares estimation for cycle-slip candidates are given as:

$$\hat{\mathbf{v}} = \mathbf{y}' - \mathbf{B}\hat{\mathbf{x}}, \quad (14)$$

where

$$\begin{aligned} \mathbf{y}' &= \mathbf{y} - \mathbf{A}\mathbf{c} \\ \hat{\mathbf{x}} &= (\mathbf{B}^T \mathbf{Q}^{-1} \mathbf{B})^{-1} \mathbf{B}^T \mathbf{Q}^{-1} \mathbf{y}'. \end{aligned} \quad (15)$$

Then, discrimination power between two candidates is measured by comparing their likelihood. We follow a conventional discrimination test procedure similar to that described by Wang *et al.* [6]. A test statistic for cycle-slip validation is given by

$$d = \Omega_{c_1} - \Omega_{c_2}, \quad (16)$$

where  $\Omega_{c_1}$  and  $\Omega_{c_2}$  are the quadratic form of the residuals of the best and second best candidates. A statistical test is performed using the following null and alternative hypotheses:

$$H_0 : E[d] = 0, \quad H_1 : E[d] \neq 0. \quad (17)$$

A test statistic for testing the above hypotheses is given by

$$W = \frac{d}{\sqrt{\text{Cov}(d)}}, \quad (18)$$

where

$$\begin{aligned} \text{Cov}[d] &= 4(\mathbf{c}_1 - \mathbf{c}_2)^T \mathbf{Q}_c^{-1} (\mathbf{c}_1 - \mathbf{c}_2) \\ \mathbf{Q}_c^{-1} &= \mathbf{Q}^{-1} - \mathbf{Q}^{-1} \mathbf{B} (\mathbf{B}^T \mathbf{Q}^{-1} \mathbf{B})^{-1} \mathbf{B}^T \mathbf{Q}^{-1}. \end{aligned} \quad (19)$$

If  $\mathbf{y}$  is assumed as having a normal distribution,  $d$  is normally distributed. Therefore,  $W$  has mean 0 and standard deviation 1 under the null hypothesis. Adopting a confidence level  $\alpha$ , it will be declared that the likelihood of the best cycle-slip candidate is significantly larger than that of the second best one if

$$W > N(0, 1; 1 - \alpha). \quad (20)$$

Finally, a reliability test is carried out after fixing cycle slips from equations (13) in order to diagnose whether errors still remain in the measurements. We will not discuss this here (see [1] and [2] for more detail).

## WORST CASE SIMULATION SCENARIOS

A reliable and fully operational cycle-slip fixing routine should operate successfully under the worst-case situations. We consider three cases: combination-insensitive cycle-slip pairings, continuous cycle slips, and low quality measurements.

### *Combination-Insensitive Cycle-Slip Pairings*

As has been reported for conventional cycle-slip fixing approaches using dual-frequency measurements ([7], [8], [9], [10] and [11]), there are particular cycle-slip pairings which cannot be readily detected in the geometry-free combination. From equation (9), the combination-insensitive cycle-slip pairings are defined as ones which satisfy the following:

$$|E[\delta\Phi_{GF}]| = |\lambda_1 \cdot \nabla\Delta C_1 - \lambda_2 \cdot \nabla\Delta C_2| \leq \varepsilon, \quad (21)$$

where  $\varepsilon$  is a threshold value which can be obtained from the second moment in equations (11). Theoretically, there are many such cycle-slip pairings. However, they can be reduced to a very small number in conjunction with equations (7).

### *Continuous Cycle Slips*

A loss of lock may be shorter than the time interval between two adjacent data collection epochs or as long as the time interval stretching over many epochs. Although the carrier phases are continuous, they are sampled during a very short time interval (e.g., 1 millisecond) in a receiver. Each of the sampled carrier phases can experience cycle slips. The carrier-phase measurements obtained under high-dynamics and at a low sampling rate may have continuous cycle slips (that is, each sequential observation is afflicted with a different cycle slip). Conventional approaches using smoothing and filtering techniques ([8], [9], [12], [13], [14], [15] and [16]) cannot handle such situations appropriately.

### *Low Quality Measurements*

Removing quasi-random errors is still a big challenge in quality control. One of the most difficult situations in fixing cycle slips is when cycle slips are mixed up with quasi-random errors. Some conventional approaches for quality control, which do not handle cycle slips separately, may have a potential problem in such situations.

## TEST RESULTS

In order to illustrate the performance of our approach, we have tested it with data sets recorded in static and kinematic modes, in short-baseline and long-baseline situations, and at low and high data rates. NovAtel OEM3 (MiLLennium), Navcom NCT-2000D and Ashtech Z-12 receivers were used to record dual-frequency data. A summary of the tests is given in Table 1.

Table 1 – Summary of the tests

	Test Mode	Approx. Baseline Length	Data Rate	Receiver Type	Doppler Frequency	Remarks
Test 1	Static	60 m	10 Hz	NovAtel OEM3	Available	Tests were conducted under the same environments: static, short-baseline and strong multipath.
Test 2	Static	60 m	10 Hz	Navcom NCT-2000D	Not available	
Test 3	Static	60 m	1 Hz	Ashtech Z-12	Available	
Test 4	Kinematic	10 m	1 Hz	Ashtech Z-12	Available	Circular motion with irregular speed
Test 5	Kinematic	80 km	1 Hz	Ashtech Z-12	Available	Driving a car at high speed

### *Verification of the Receiver Clock Jumps*

Two typical examples of receiver clock jumps are illustrated in Figures 2 and 3. The first example is a millisecond jump which occurred in the Ashtech Z-12 as seen in Figure 2. The top panel shows the receiver clock offsets estimated by the C/A-code pseudoranges and reveals that the millisecond jumps occurred about every 7 minutes. As was explained in the section “Receiver Clock Jumps”, the effects on the geometric range corresponding to the jumps are removed in the DD measurements. However, the effects on the geometric range rate corresponding to the jumps still remain in the DD measurements. The spikes in the TD time series, as seen in the middle and bottom panels, disclose the significance of such effects. Using the Doppler frequency, such effects can be easily estimated and removed. The second example is a very small

clock jump which occurred in the Navcom NCT-2000D as seen in Figure 3. The top panel shows the receiver clock offset estimates including the microsecond-level jumps which occur every second. Since the jumps are so small, the effects of the geometric range rate corresponding to the jumps seem to be buried in the noise of the TD measurements; *i.e.*, the TD time series would not reveal the spikes as verified in the middle and bottom panels. However, it should be noted that such effects could reach the level of a few centimetres when a satellite is close to the horizon and at the same time the receiver experiences high dynamics. Without correcting for such effects, we may have difficulty in fixing cycle slips and subsequently, in overall quality control of the carrier-phase measurements.

### Tuning the Parameters for Cycle-Slip Candidates

Two parameters are involved in examining cycle-slip candidates in our approach. The threshold of the TD geometry-free phase,  $\epsilon_{GF}$ , is used in filtering cycle-slip candidates while that of the TD prediction residuals,  $\epsilon_{CS}$ , is used in generating the candidates. Figures 4 and 5 show two typical examples of the parameters which are tuned for the cycle-slip candidates. The examples were taken from Test 1 (static, short-baseline, high data rate) and Test 5 (kinematic, long-baseline, low data rate), respectively. Assuming that the systematic errors such as the receiver clock jumps and cycle slips are removed in the carrier-phase measurements, the parameters reflect the combined effects of the biases and receiver system noise. As a result, they are highly dependent on the receiver type and test environments. This means that we need to tune the parameters either via calibration or adaptive estimation. The examples not only highlight this requirement, but also reveal the quasi-random characteristic of the biases and noise. One crucial use of the quasi-random characteristic of the biases and noise is employing their second moments to set the threshold values in limiting the range of cycle-slip candidates and filtering the candidates.

The estimates of the parameters are summarized in Table 2. After removing the systematic errors in the measurements for each data set, one thousand epochs of measurements were used to estimate the parameters. Assuming that the combined effects of the biases and noise follow a normal distribution, the confidence level of the estimates in Table 2 corresponds to 99.7% (*i.e.*,  $k = 3$ ). For example, given the values of the TD prediction residuals at a certain epoch in Test 5, the probability that the cycle-slip candidates in the range of  $\pm 1$  cycle (about 19 cm and 24 cm for L1 and L2, respectively) centred at the given TD values include the true cycle-slip values is over 99.7%. Setting  $\epsilon_{GF}$  to 1 cm in the example, the probability that the candidates passing the threshold test in equations (12) include the true cycle-slip values is over 99.7%.

Table 2 – Estimates of the parameters for cycle-slip candidates ( $k = 3$ ) (mm)

	Test 1			*Test 2			Test 3			Test 4			Test 5		
	mean	$\sigma$	rms	mean	$\sigma$	rms	mean	$\sigma$	rms	mean	$\sigma$	rms	mean	$\sigma$	rms
$\epsilon_{GF}$	0.2	4.5	4.5	0.0	16.6	16.6	0.0	4.5	4.5	0.0	9.6	9.6	-0.2	7.6	7.6
$\epsilon_{CS_1}$	0.3	16.5	16.5	-1.5	186.9	186.9	0.0	5.7	5.7	-0.3	271.5	271.5	0.0	142.2	142.2
$\epsilon_{CS_2}$	0.3	16.8	16.8	-1.5	187.5	187.5	0.0	7.2	7.2	-0.3	271.5	271.5	0.3	143.1	143.1

\*Compared with the estimates of Test 1 and 3, those of Test 2 are noisier because the Doppler frequency was not available in Test 2.

### Verification of Quasi-Random Errors

Quasi-random errors such as multipath, diffraction, ionospheric scintillation, *etc.* usually make it difficult to fix cycle slips correctly. Since the cycle slip constraint of discontinuities of an integer number of cycles does not apply to quasi-random errors, fixing cycle slips is a big challenge when systematic and quasi-random errors are interspersed. One typical example of signal diffraction due to obstructions is illustrated in Figures 6 through 8. The example was taken from Test 3. Figure 6 shows that one satellite (PRN 21) was temporarily (for about 2 minutes) blocked by the penthouse on the roof of Gillin Hall at UNB. (Head Hall data acquired during the period of obstruction on Gillin Hall has been deleted in the bottom panel) Rapid signal degradation at the moment of signal obstruction as seen in the middle panel implies that there could be significant deterioration in the quality of the measurements. On the other hand, Figure 7 shows that the other satellite (PRN 27), which was used with PRN 21 in generating the DD measurements, did not suffer from such effects. This appears to confirm that the spikes in the TD measurements seen in Figure 8 were due to signal diffraction.

Two numerical examples are given in Figure 8 to explain how our approach handles such situations. Two pairs of the TD L1 and L2 measurements, the points A1 and A2, and B1 and B2, were obtained at elapsed time 76 and 78 seconds, respectively. Firstly, we generated cycle-slip candidates for each pair using the parameter estimates of Test 3 in Table 2. Then the threshold test in equations (12) was carried out to filter the candidates. We outline the result in Table 3. Since there is no cycle-slip candidate which passes the threshold test, we can conclude that at the 99.7% confidence level the spikes in Figure 8 are not cycle slips. It should be noted that the validation test described in the section "Cycle-Slip Validation" should

be performed if more than one cycle-slip candidate passes the threshold test. A conventional quality control procedure (e.g., data snooping) follows the cycle-slip correction routine to identify and remove the problematic measurements.

Table 3 – Filtering the cycle-slip candidates ( $\epsilon_{GF} = 4.5$  when  $k = 3$ )

	A1 and A2		B1 and B2	
	L1	L2	L1	L2
CS Candidates (cycles)	1	1	1	1
$CS' = \lambda_1 \cdot CS_1 - \lambda_2 \cdot CS_2$ (mm)	-50		-50	
TD Measurements (m/sec)	191	195	110	140
$\delta\Phi_{GF} = \delta\nabla\Delta\Phi_1 - \delta\nabla\Delta\Phi_2$ (mm)	-4		-30	
$ CS' - \delta\Phi_{GF} $ (mm)	46		20	
Threshold Test Result	Not passed		Not passed	

### Instantaneous Cycle-Slip Correction Performance

We have tested our approach using data sets recorded in a variety of situations. Two aspects have stood out in the tests. First, the approach is capable of instantaneous cycle-slip correction. This means that it is suitable for real-time applications, not only for post-processing. Second, the approach can handle cycle slips in low quality measurements. Unlike conventional approaches, therefore, we do not have to discard the measurements obtained at low elevation angles and from weak signals with low  $C/N_0$  values. As a result, our approach tends to increase observation redundancy and hence system performance (e.g., integrity, continuity, accuracy and availability) is improved. A typical example which shows the performance of our approach is illustrated in Figures 9 through 11. Figures 9 and 10 show the two satellites which were used in generating the DD measurements. They were observed more or less at high elevation angles. However, the signal of one satellite (PRN 8) was heavily affected by what appears to be ground-bounce multipath as seen in Figure 9. While the L1 signal was still fairly strong in such situations, the L2 signal was fading quickly and automatic gain control attempted to compensate for the low gain situation. As a result, we can see L2/P2  $C/N_0$  gain jumps in the middle and bottom panels. Figure 11 shows that the L1 and L2 TD measurements were contaminated by many cycle slips (the first and third panels) and confirms that our approach fixed them perfectly (the second and fourth panels).

### Worst Case Simulation Test

A simulation test was carried out to confirm the performance of our approach under worst-case scenarios. Firstly, we selected a data set which was recorded under high dynamics and in an abundant ground-bounce multipath environment. Fixing cycle slips in such situations is still a big challenge. A typical example of such situations is illustrated in Figures 12 and 13. Figure 12 shows that there was frequent irregular maneuvering while recording the data. High dynamics can be evidenced by jerks due to circular motion with irregular speed. This data set was collected during Test 4. The middle and bottom panels in Figure 13 indicate that the rover was experiencing severe signal degradation due to multipath and receiver system noise during the test. Pre-processing was conducted to detect and correct the systematic errors such as receiver clock jumps and cycle slips. After fixing the systematic errors, we used the data in the simulation test. We then simulated cycle slips which represent the most combination-insensitive cycle-slip pairing: the nine-to-seven combination of L1 and L2 phases in cycle units. The effect of such a combination in the TD geometry-free phase is only 3.2 mm ( $\approx 9 \cdot \lambda_1 - 7 \cdot \lambda_2$ ), this value being too small to be filtered by the threshold test in equations (12). This combination was multiplied by randomly selected integer numbers in the range [-5,5] continuously for 100 seconds and added to the original data. We also selected the worse place to simulate cycle slips – they were put in the middle of the circular motion portion of the data set (elapsed time 700 to 800 seconds) as seen in Figure 14. The simulated cycle slips reflect exactly what we have described in the section "Worst Case Simulation Scenarios". Furthermore, we introduced more difficult situations in the simulation test. Figure 15 shows the entire collection of cycle slips simulated simultaneously for *all* satellites. This additional condition was also considered for the completeness of our approach. Figure 16 shows an example of cycle-slip recovery for this simulation. The result was compared with the original cycle-slip-free data set in Figure 12. It was confirmed that our approach performed perfectly in the given situations. As a matter of fact, the simulated cycle slips for all satellites were correctly recovered simultaneously.

A numerical example which shows a snapshot result of our approach is summarized in Tables 4 and 5. The simulated cycle slips and TD measurements for all DD satellite pairs at elapsed time 700 seconds are given in Table 4. Using the parameter estimates of Test 4 in Table 2, we generated and filtered cycle-slip candidates for each pair according to equations (8) and (12), respectively. We purposely used an almost 100% confidence level ( $k = 10$ ) in this example. As seen in the bottom row of Table 4, more than one pair of cycle-slip candidates passed the threshold test in equations (12). Accordingly,

we carried out the validation test described in the section "Cycle-Slip Validation". We outline the result in Table 5. The first and second best combinations of the candidates which minimize the quadratic form of the residuals were obtained and then the discrimination power between them was measured statistically. Assuming that the combined effects of the biases and noise in the carrier-phase measurements follow the normal distribution, the  $W$ -estimate in Table 5 represents the threshold-to-noise variance ratio of the standard normal distribution function. Therefore, we can be assured at an almost 100% confidence level that the first best combination represents the true cycle-slip values in this example. This confirms that our approach recovered the simulated cycle slips correctly.

Table 4 – Filtering the cycle-slip candidates ( $\epsilon_{GF} = 32$ ,  $\epsilon_{CS_1} = 905$ ,  $\epsilon_{CS_2} = 905$  when  $k = 10$ )

		DD Pairs (PRN 1/PRN 2)								
		23/3	3/28	28/1	1/25	25/13	13/19	19/31	31/15	15/17
Simulated CS (cycles)	L1	-9	9	18	9	27	9	18	-18	0
	L2	-7	7	14	7	21	7	14	-14	0
TD Measurements (m/sec)	L1	-1.582	1.537	3.121	1.272	5.431	1.336	3.060	-3.874	0.368
	L2	-1.569	1.541	3.123	1.273	5.432	1.337	3.056	-3.865	0.372
CS Candidates (cycles)	L1	-13 -9 -4	9 14	14 18 23	9 14	23 27 32	9	18	-18	0
	L2	-10 -7 -3	7 11	11 14 18	7 11	18 21 25	7	14	-14	0

Table 5 – Cycle-slip validation

		First Best Combination	Second Best Combination
L1	CS Candidates	-9 9 18 9 27 9 18 -18 0	-4 14 23 14 32 9 18 -18 0
	$\Omega_c$	2.8	11004.0
	$d$	11001.2	
	$W$	13.2	
L2	CS Candidates	-7 7 14 7 21 7 14 -14 0	-3 11 18 11 25 7 14 -14 0
	$\Omega_c$	3.9	11523.0
	$d$	11519.1	
	$W$	14.7	

## CONCLUSION

Over the past decade, a number of methods have been developed to handle errors in the carrier-phase measurements. There are, in large, two main research streams in this area: cycle-slip-related research and quality-control-related research. The former focuses mainly on cycle slips and takes advantage of the systematic characteristics of cycle slips, more or less ignoring the effects of the other errors. As a matter of fact, cycle slips are the biggest error source if they remain in the carrier-phase measurements. On the other hand, the latter approach considers that all biases and errors must be detected by a rigorous statistical test such as the reliability test. This approach tends more or less not to utilize the advantage taken by the former. We use a hybrid method for quality control: systematic errors such as cycle slips and receiver clock jumps are examined and corrected first; then, a reliability test is carried out to reduce the effects of quasi-random errors.

Three main features differentiate our approach from conventional techniques. First, our approach is suitable for kinematic applications either in real-time or in post-processing mode. Unlike conventional approaches such as a sequential least-squares estimator or Kalman filter which uses the prediction values of the measurements for quality control, our approach does not require them. Instead, it utilizes only the current epoch's measurements for quality control. Therefore, the approach can attain high performance even when a receiver platform is maneuvering. Second, the approach can handle cycle slips in low quality measurements, so that we do not have to discard the measurements obtained at low elevation angles and from weak signals with low  $C/N_0$  values. As a result, the approach tends to increase observation redundancy and hence system performance in terms of integrity, continuity, accuracy and availability is improved. Third, the approach enables us to determine system performance by simply assigning the confidence level of the parameters for cycle-slip candidates when designing the system.

Tests carried out in a variety of situations including static and kinematic modes, short-baseline and long-baseline situations, and low and high data rates have confirmed the high performance of our approach. A worst-case simulation test has also proved its performance. However, we are aware that the same generic (intrinsic) limitations as with least-squares estimation still remain in our approach; *i.e.*, the need for redundancy and stochastic modelling. To increase redundancy, we need to use as many measurements as are available in real world scenarios. In this case, many problematic situations can occur in the measurements, particularly ones obtained at low elevation angles and from weak signals with low  $C/N_0$  values. As mentioned previously, our approach indeed works well in such situations. Finally, statistical testing and reliability analysis can only be efficient if the stochastic models are correctly known or well approximated. Obtaining a reliable stochastic model is still a big challenge. However, the “differencing-in-time” method described in one of our previous papers [17] has been successfully tested and implemented in our approach.

## ACKNOWLEDGEMENTS

The research reported in this paper was conducted under the program of the GEOIDE Network of Centres of Excellence (Project ENV#14). The support of the Canadian Coast Guard; the Canadian Hydrographic Service; VIASAT Géo-Technologie Inc.; Geomatics Canada; NovAtel Inc.; and the Centre de Recherche en Géomatique, Université Laval is gratefully acknowledged. The authors would like to thank Sunil B. Bisnath (currently a Ph.D. candidate at UNB) for his review of a draft of this paper and for his insightful comments.

This paper is based, in part, on a paper [18] presented at the International Symposium on Kinematic Systems in Geodesy, Geomatics and Navigation, held in Banff, Alberta, Canada in June 2001.

## REFERENCES

1. Leick, A., *GPS Satellite Surveying*, 2nd edition, John Wiley and Sons, Inc., 1995.
2. Teunissen, P.J.G. and A. Kleusberg (editors), *GPS for Geodesy*, 2nd edition, Springer-Verlag, 1998.
3. Rizos, C., *Quality Issues in Real-time GPS Positioning*, Final Report of the IAG SSG 1.154, July 1999, (Available on-line at: <[http://www.gmat.unsw.edu.au/ssg\\_RTQC/ssg\\_rtqc.pdf](http://www.gmat.unsw.edu.au/ssg_RTQC/ssg_rtqc.pdf)>).
4. Baarda, W., *A Testing Procedure for Use in Geodetic Networks*, Publications on Geodesy, New Series, Vol. 2, No. 5, Netherlands Geodetic Commission, 1968.
5. Hofmann-Wellenhof, B., H. Lichtenegger, and J. Collins, *GPS Theory and Practice*, 4th edition, Springer-Verlag, 1997.
6. Wang, J., M. P. Stewart and M. Tsakiri, *A discrimination test procedure for ambiguity resolution on-the-fly*, Journal of Geodesy, Vol. 72, No. 11, 1998, pp. 644-653.
7. Goad, C., *Precise positioning with the Global Positioning System*, Proceedings of the Third International Symposium on Inertial Technology for Surveying and Geodesy, Banff, Canada, 16-20 September 1985, pp. 745-756.
8. Bastos, L. and H. Landau, *Fixing cycle slips in dual-frequency kinematic GPS-applications using Kalman filtering*, Manuscripta Geodaetica, Vol. 13, No. 4, 1988, pp. 249-256.
9. Blewitt, G., *An automatic editing algorithm for GPS data*, Geophysical Research Letters, Vol. 17, No. 3, 1990, pp. 199-202.
10. Gao, Y. and Z. Li, *Cycle slip detection and ambiguity resolution algorithms for dual-frequency GPS data processing*, Marine Geodesy, Vol. 22, No. 4, 1999, pp. 169-181.
11. Bisnath, S.B., *Efficient, automated cycle-slip correction of dual-frequency kinematic GPS data*, Proceedings of ION GPS 2000, Salt Lake City, Utah, 19-22 September 2000, pp. 145-154.
12. Lichtenegger, H. and B. Hofmann-Wellenhof, *GPS-data preprocessing for cycle-slip detection*, International Association of Geodesy Symposium 102, Edinburgh, Scotland, 2-8 August 1989, pp. 57-68.
13. Kleusberg, A., Y. Georgiadou, F. van den Heuvel, and P. Heroux, *GPS Data Preprocessing with DIPOP 3.0*, internal technical memorandum, Department of Geodesy and Geomatics Engineering, University of New Brunswick, Fredericton, Canada, 1993.
14. Collin, F. and R. Warnant, *Application of the wavelet transform for GPS cycle slip correction and comparison with Kalman filter*, Manuscripta Geodaetica, Vol. 20, No. 3, 1995, pp. 161-172.
15. Han, S., *Carrier Phase-based Long-range GPS Kinematic Positioning*, UNISURV S-49, School of Geomatic Engineering, The University of New South Wales, Sydney, N.S.W., Australia, 1997.
16. Bisnath, S.B., D. Kim and R.B. Langley, *A new approach to an old problem: carrier-phase cycle slips*, GPS World, Vol. 12, No. 5, May 2001, pp. 46-51.

17. Kim, D. and R.B. Langley, *Estimation of the stochastic model for long-baseline kinematic GPS applications*, Proceedings of The Institute of Navigation 2001 National Technical Meeting, Long Beach, CA, U.S.A., 22-24 January 2001, pp 586-595.
18. Kim, D. and R.B. Langley, *Instantaneous real-time cycle-slip correction of dual-frequency GPS data*, Proceedings of the International Symposium on Kinematic Systems in Geodesy, Geomatics and Navigation, Banff, Alberta, Canada, 5-8 June 2001, pp. 255-264.

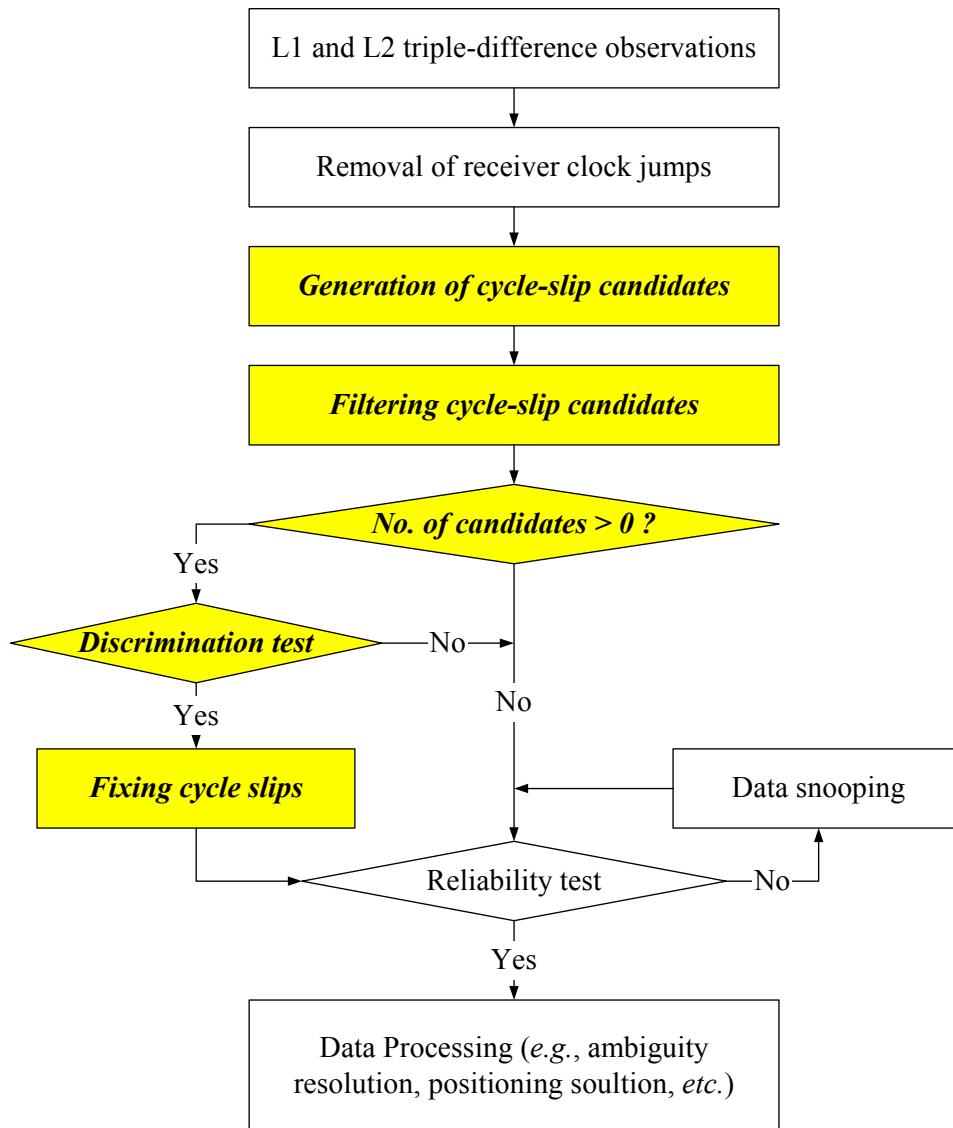


Fig. 1 – Quality control of the carrier-phase measurements in conjunction with an instantaneous cycle-slip correction routine (steps labelled in italics).

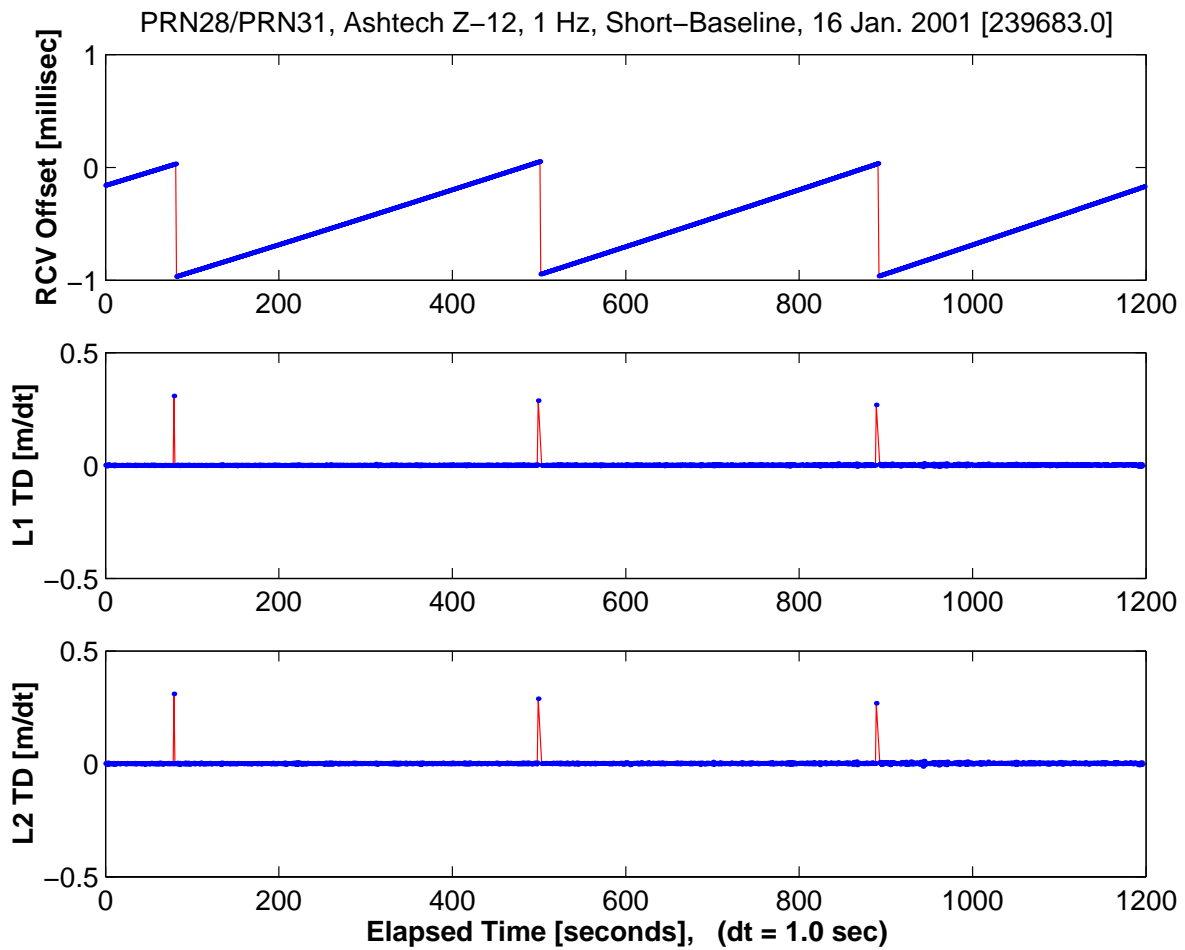


Fig. 2 – Effects of the receiver clock jumps (Ashtech Z-12, Test 3): the receiver clock offset estimates (top); and the L1 and L2 TD measurements disclosing the effects of the geometric range rate corresponding to the jumps (middle and bottom). The number in square brackets is the GPS Time of first observation. Vertical axis scale for TD values is normalized using the observation sampling interval ( $dt$ ).

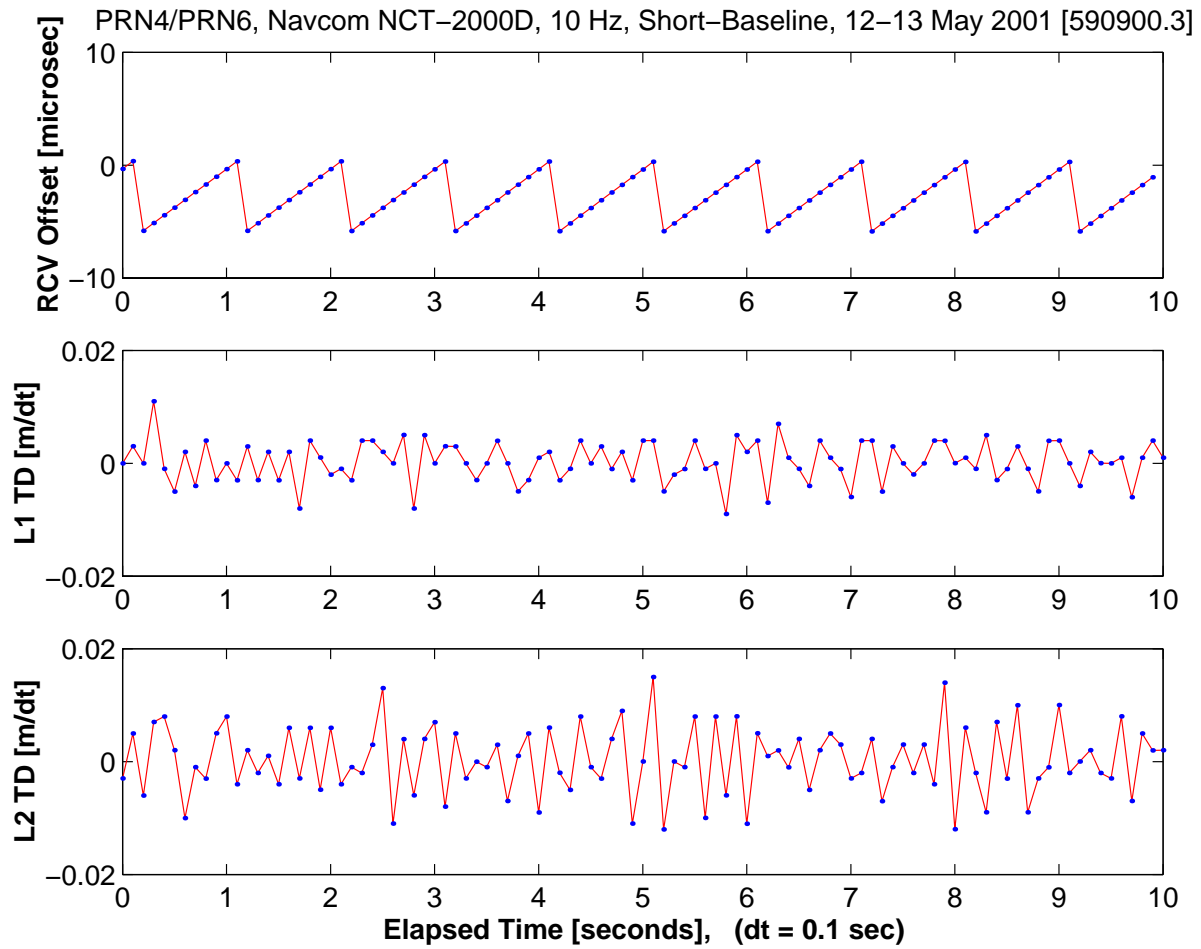


Fig. 3 – Effects of the receiver clock jumps (Navcom NCT-2000D, Test 2): the receiver clock offset estimates (top); and the L1 and L2 TD measurements hiding the effects of the geometric range rate corresponding to the jumps (middle and bottom).

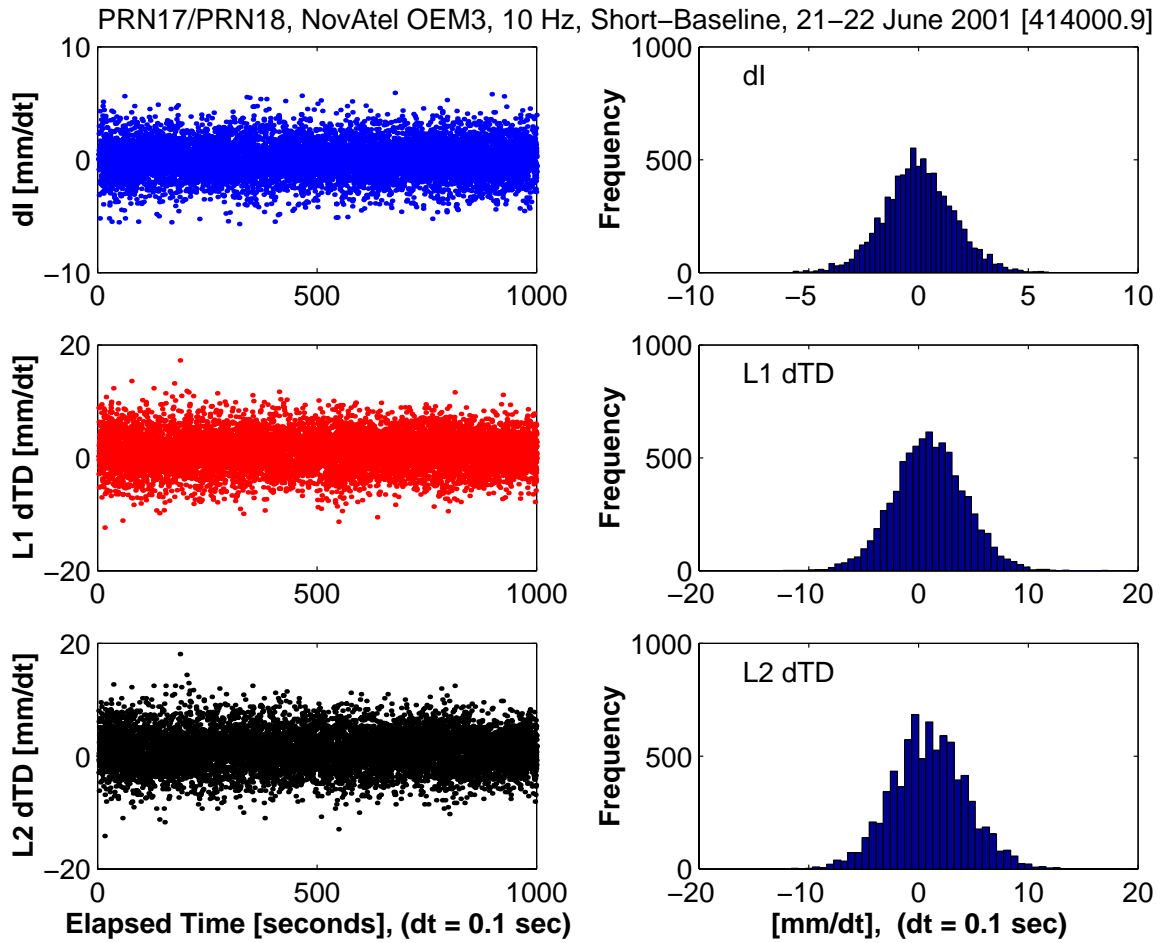


Fig. 4 – Tuning the parameters for cycle-slip candidates (Test 1): a scaled version of the TD geometry-free phase where  $dI = \delta\Phi_{GF}/(\gamma-1)$  (top); and the TD prediction residuals of L1 and L2 where  $dTD = \delta\Phi_{TD}$  (middle and bottom).

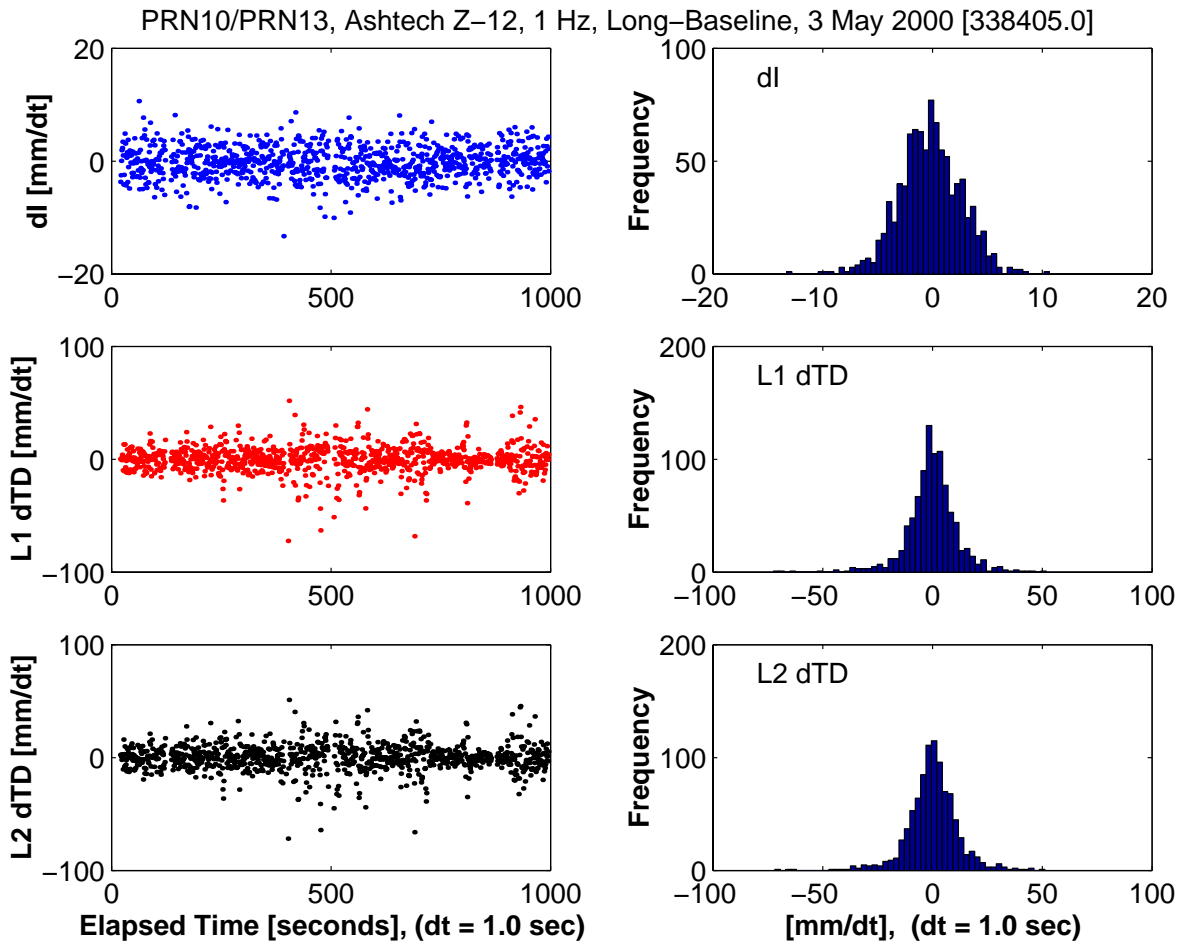


Fig. 5 – Tuning the parameters for cycle-slip candidates (Test 5): a scaled version of the TD geometry-free phase where  $dI = \delta\Phi_{GF}/(\gamma-1)$  (top); and the TD prediction residuals of L1 and L2 where  $dTD = \delta\Phi_{TD}$  (middle and bottom).

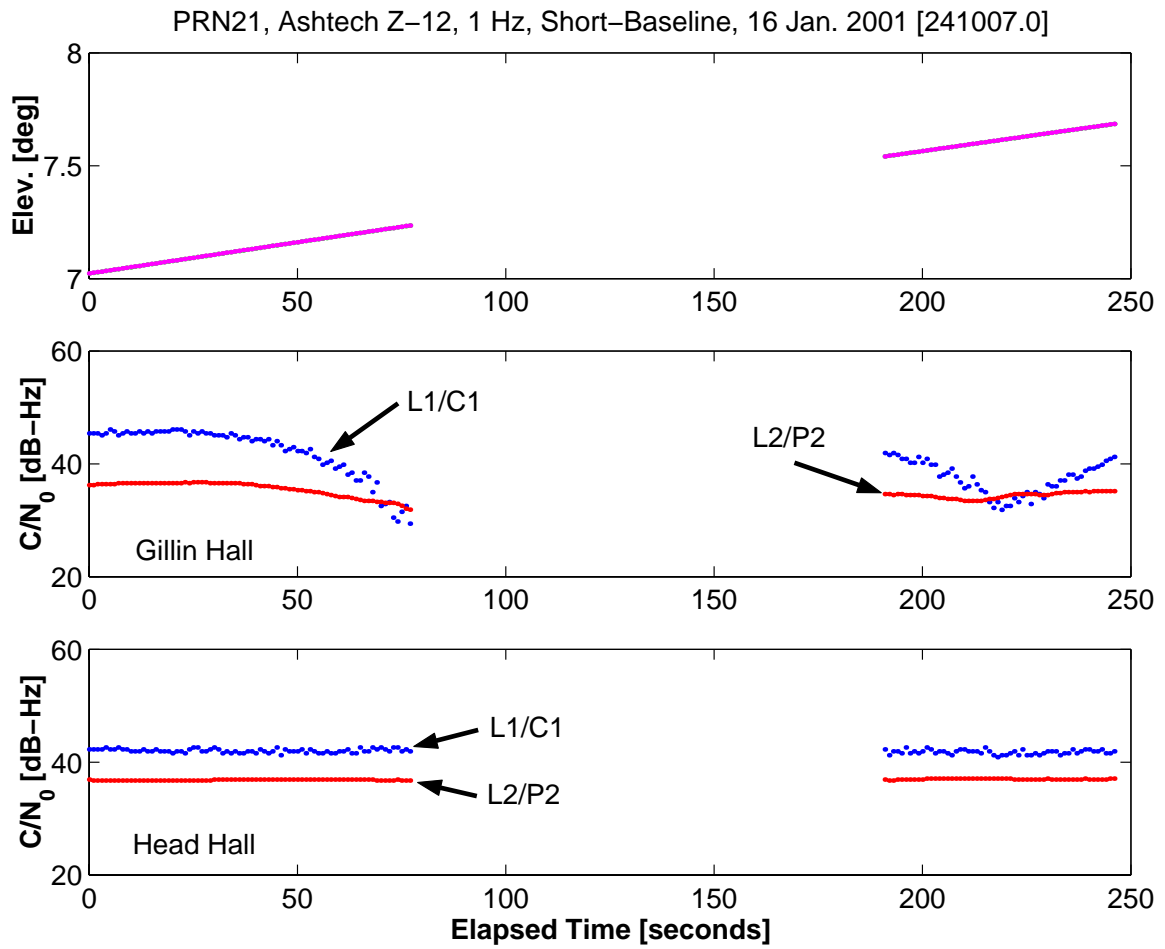


Fig. 6 – Signal degradation due to diffraction (middle) (Test 3).

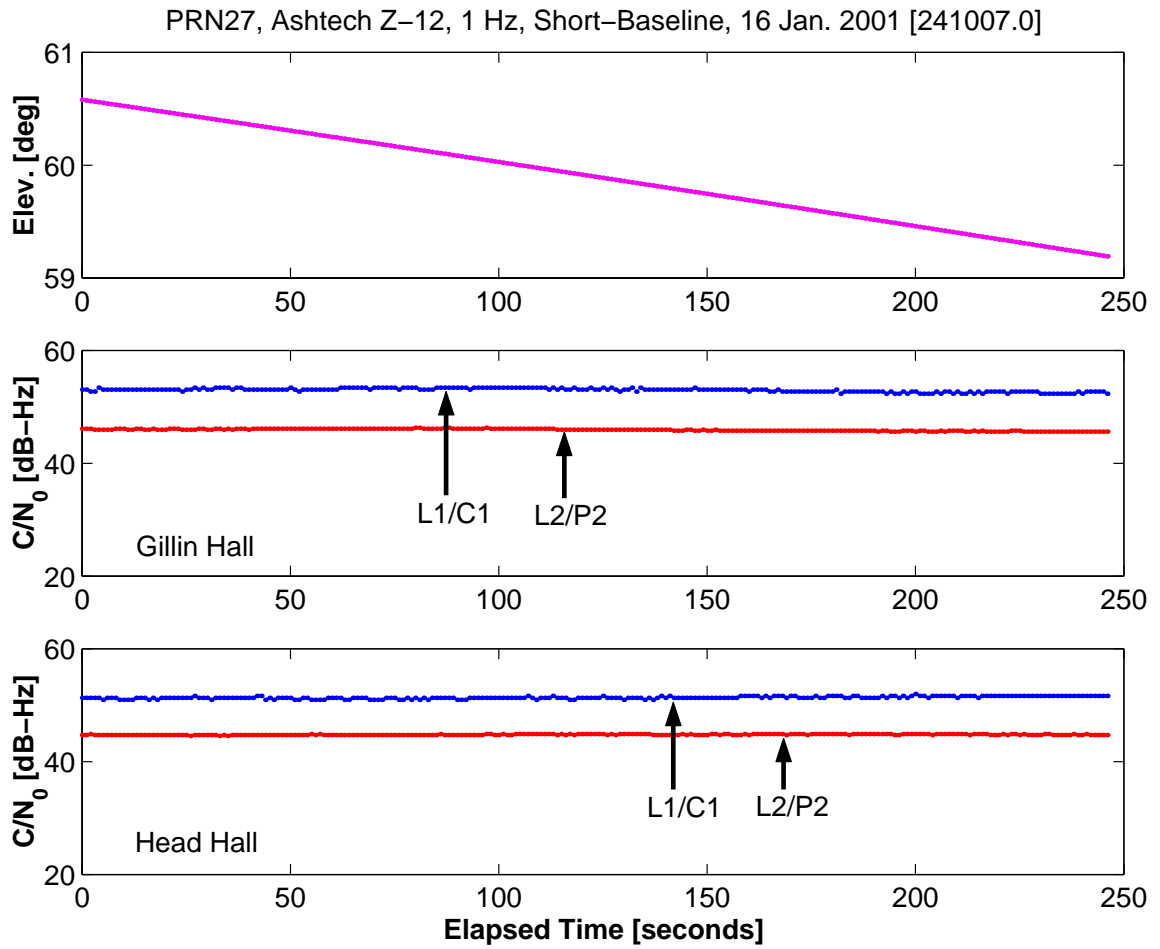


Fig. 7 – Normal (i.e., not problematic) signal reception situations confirmed by the satellite elevation angles and  $C/N_0$  values (Test 3).

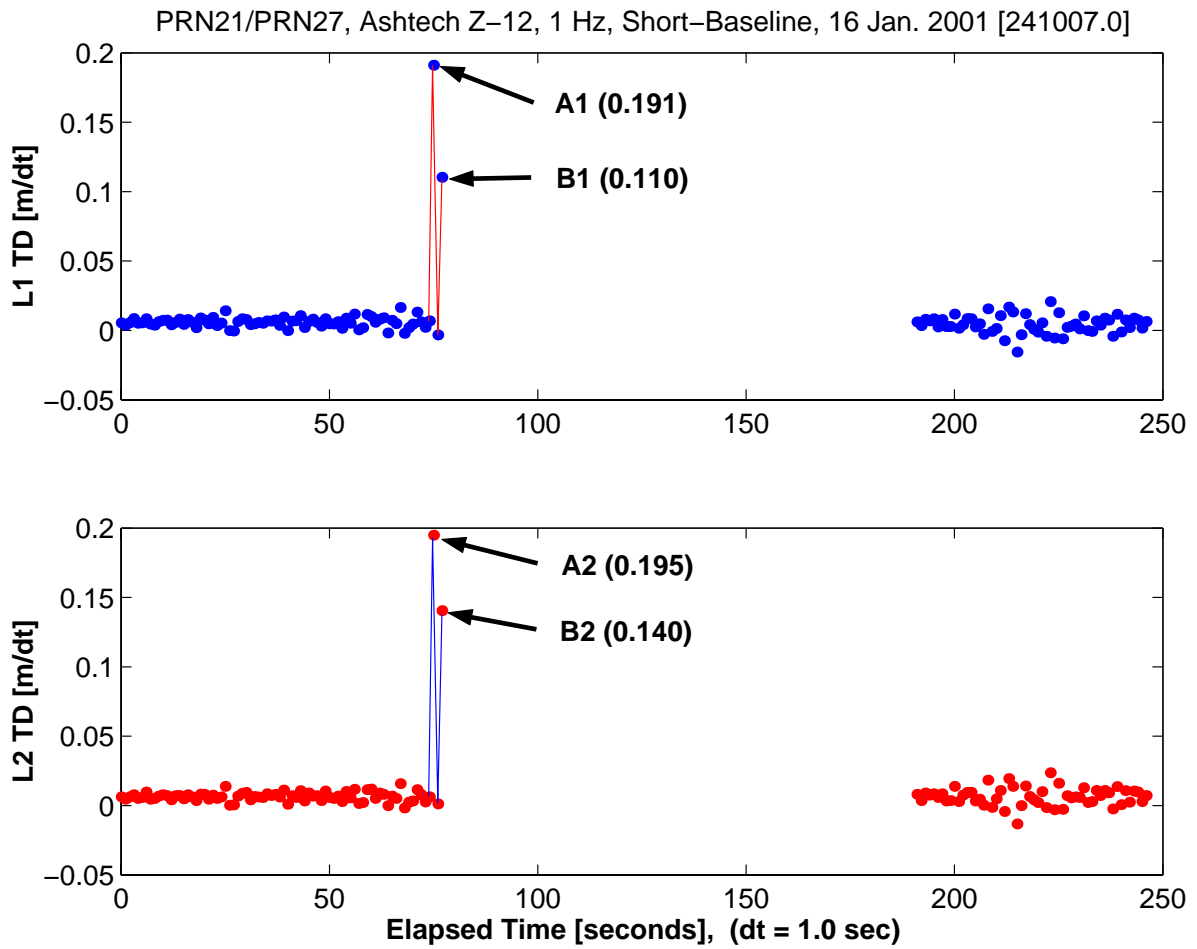


Fig. 8 – Effects of signal diffraction in the L1 and L2 TD measurements (Test 3).

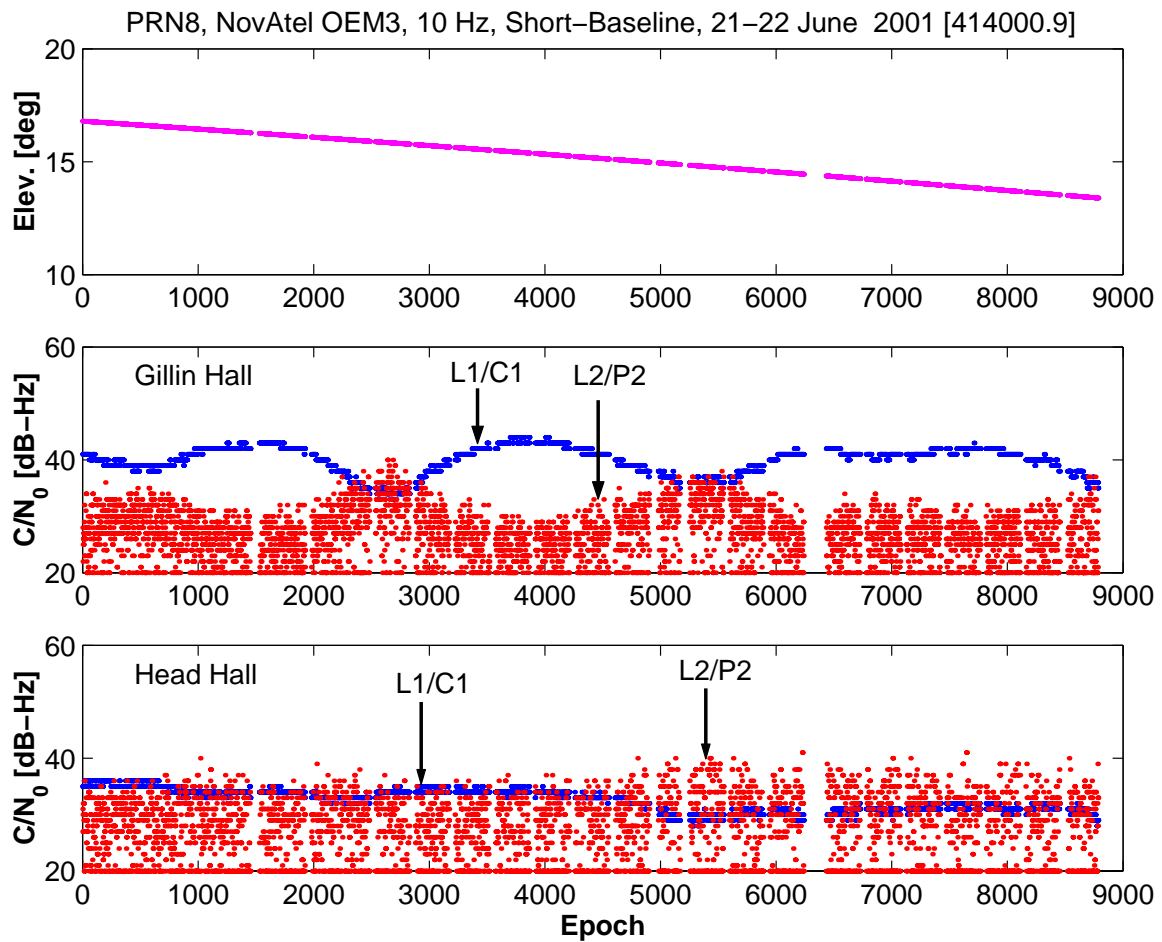


Fig. 9 – Signal degradation due to multipath (Test 1).

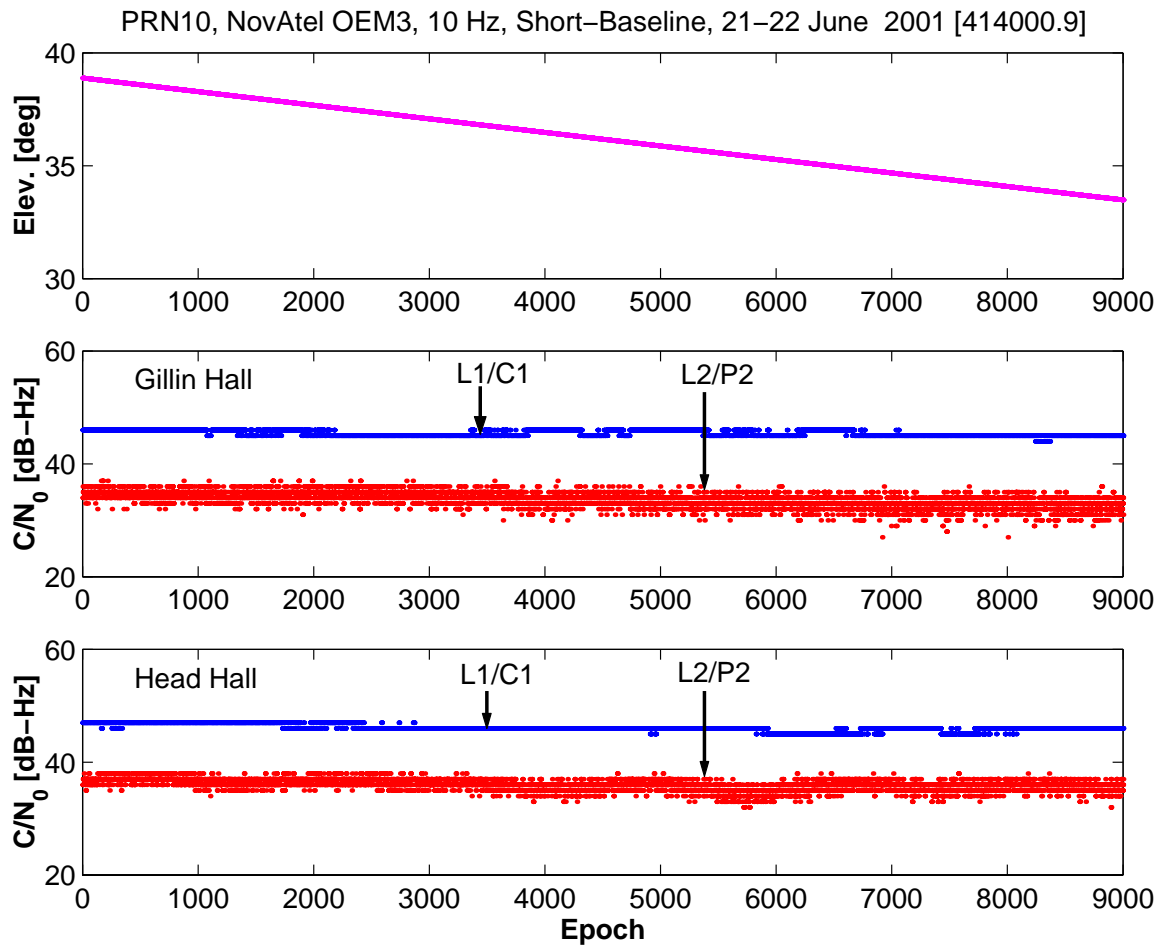


Fig. 10 – Normal (i.e., not problematic) signal reception situations confirmed by the satellite elevation angles and  $C/N_0$  values (Test 1).

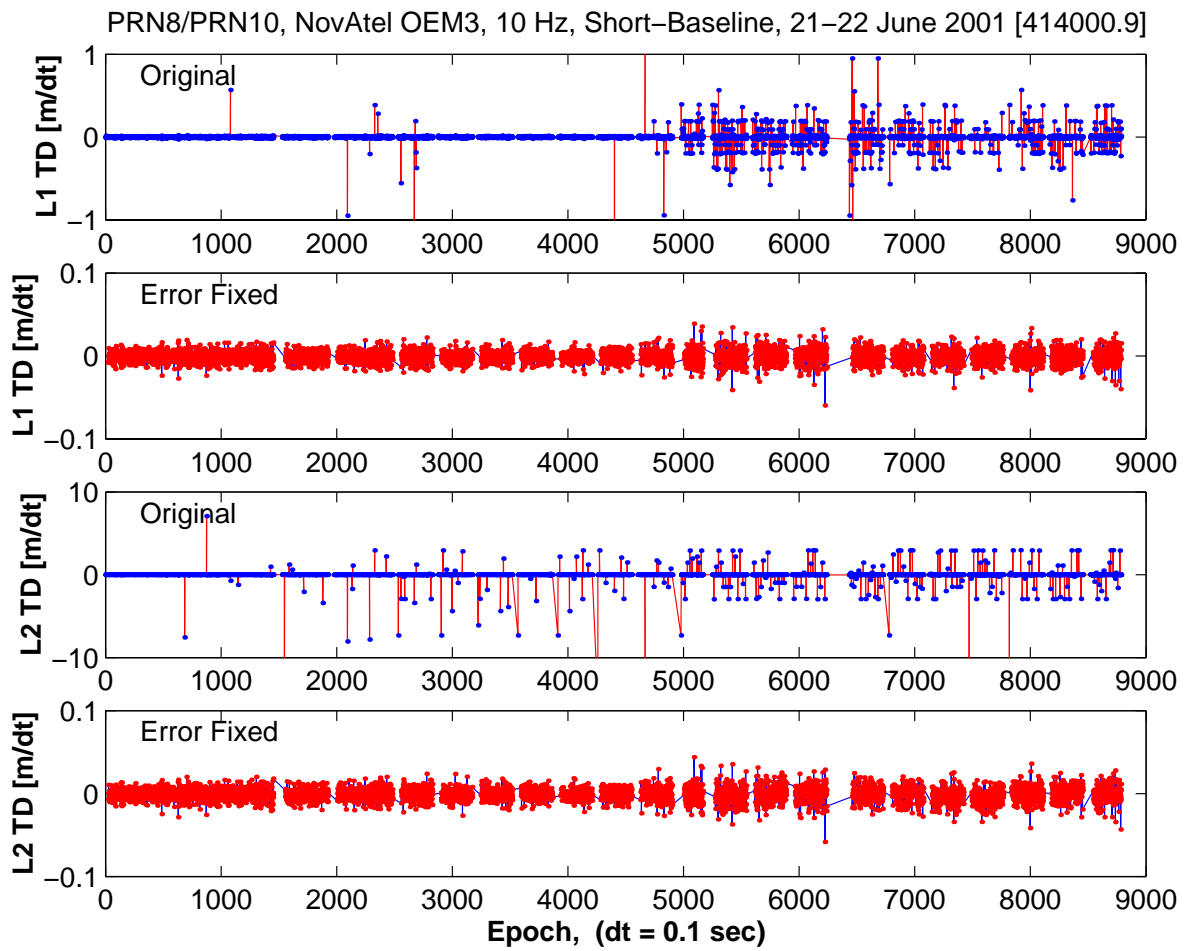


Fig. 11 – Performance of instantaneous cycle-slip correction.

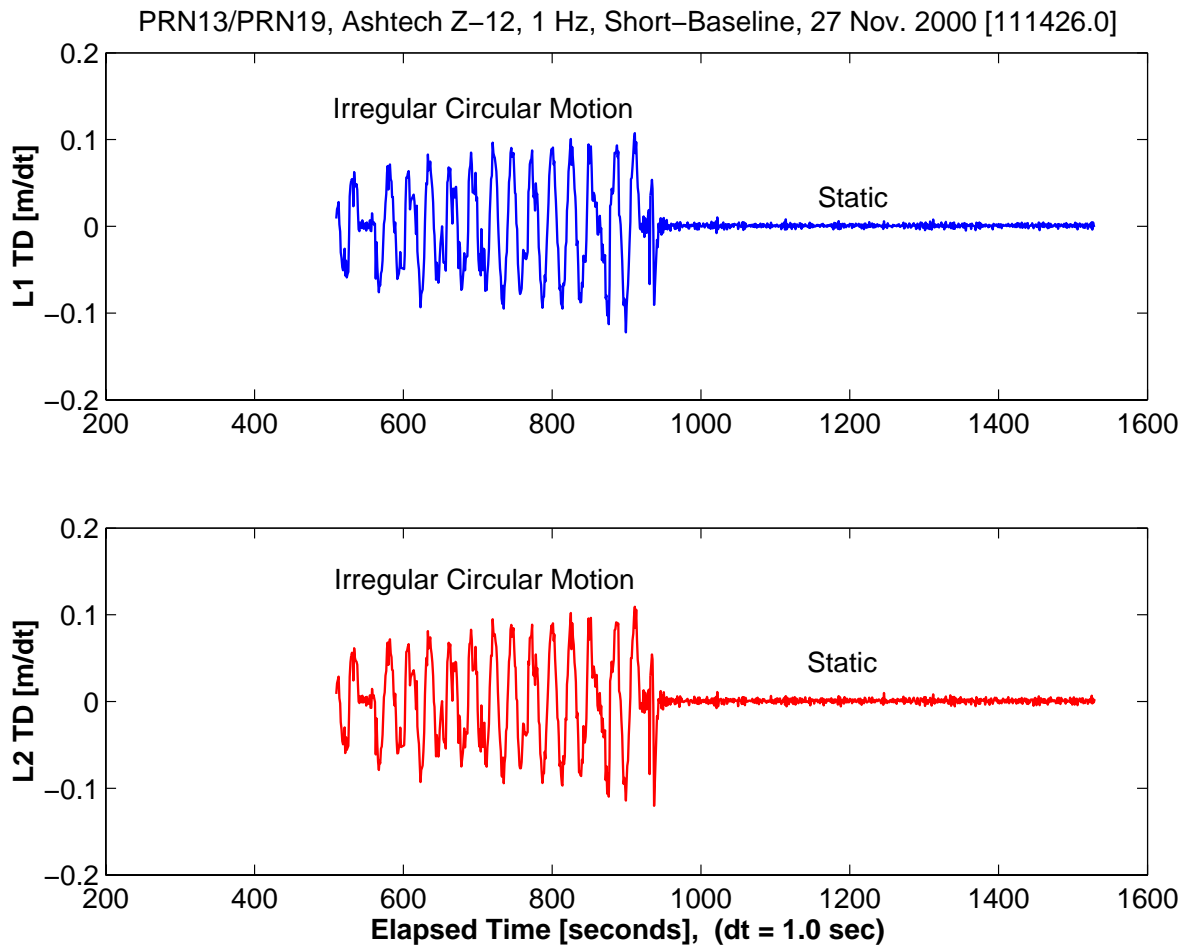


Fig. 12 – Data set obtained in high dynamics scenario (Test 4).

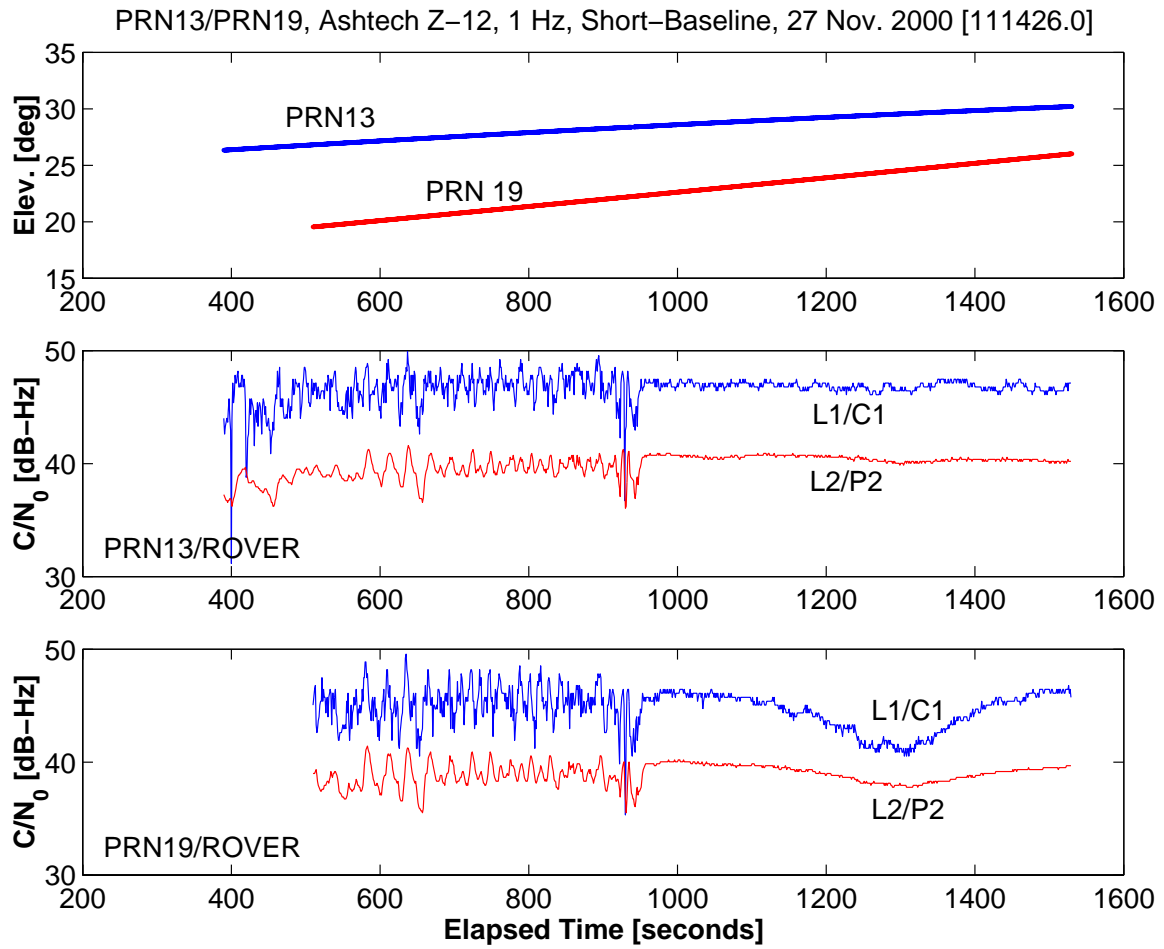


Fig. 13 – Signal degradation due to multipath and receiver dynamics (Test 4).

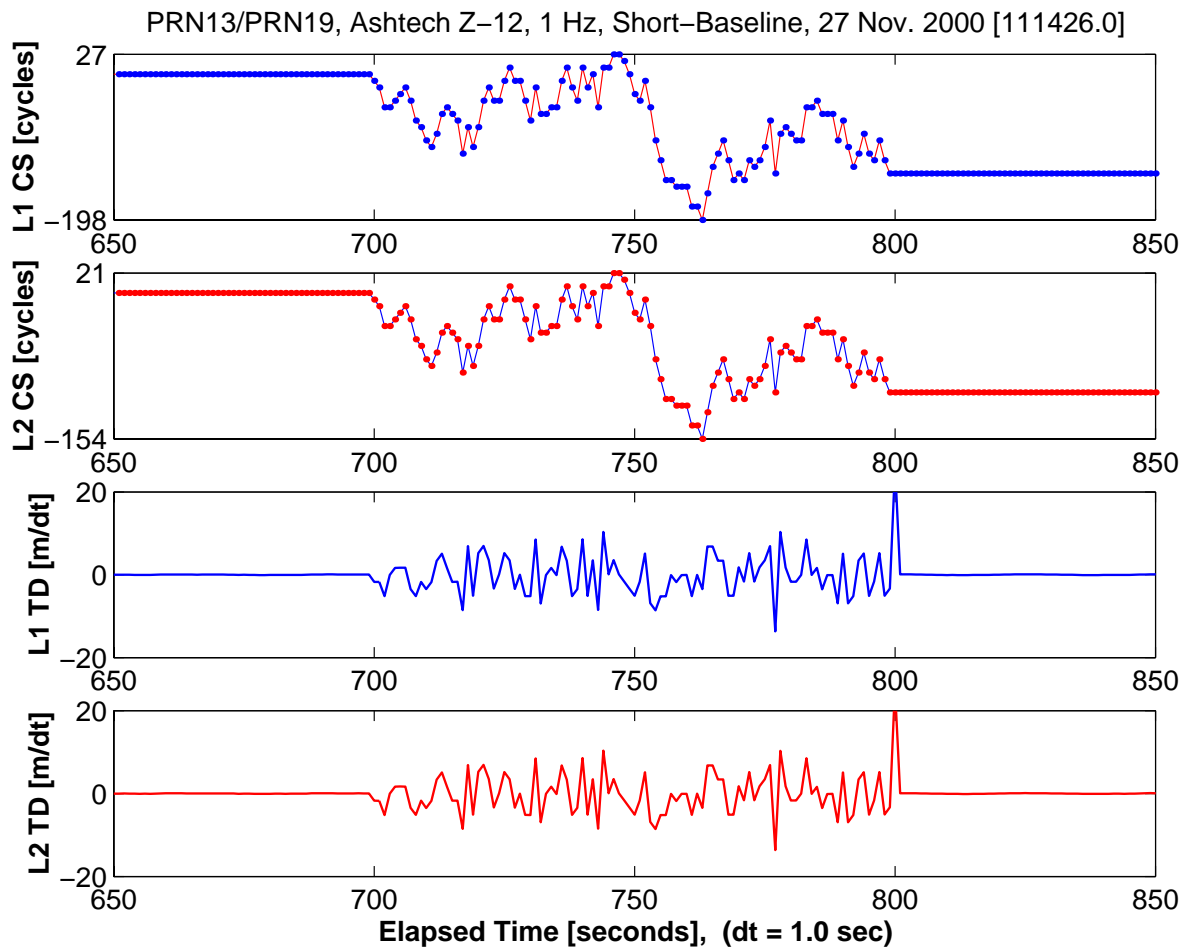


Fig. 14 – Simulated (accumulated) L1 and L2 cycle slips (the top two panels), and the TD L1 and L2 measurements containing them (the bottom two panels) (Test 4).

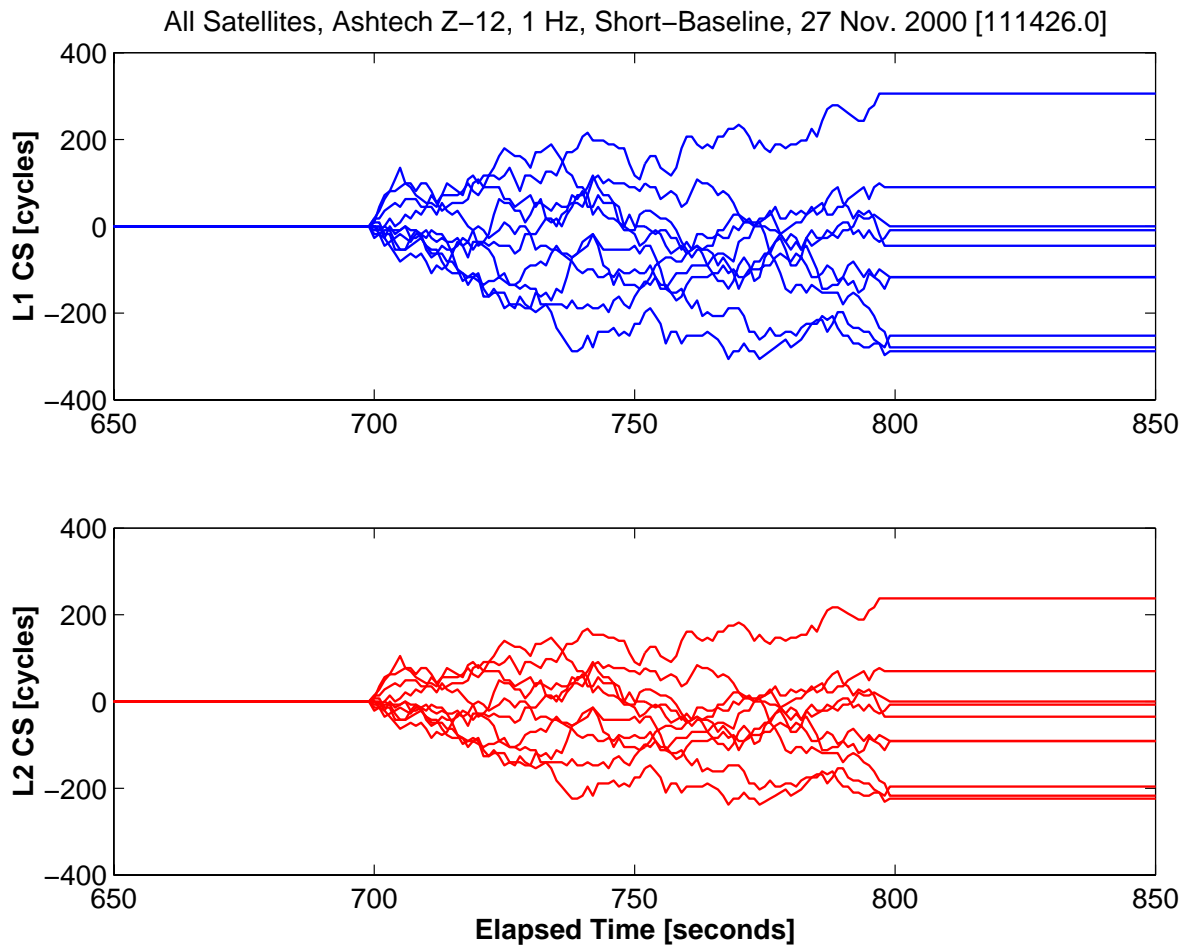


Fig. 15 – Simulated (accumulated) L1 and L2 cycle slips for all satellites (Test 4).

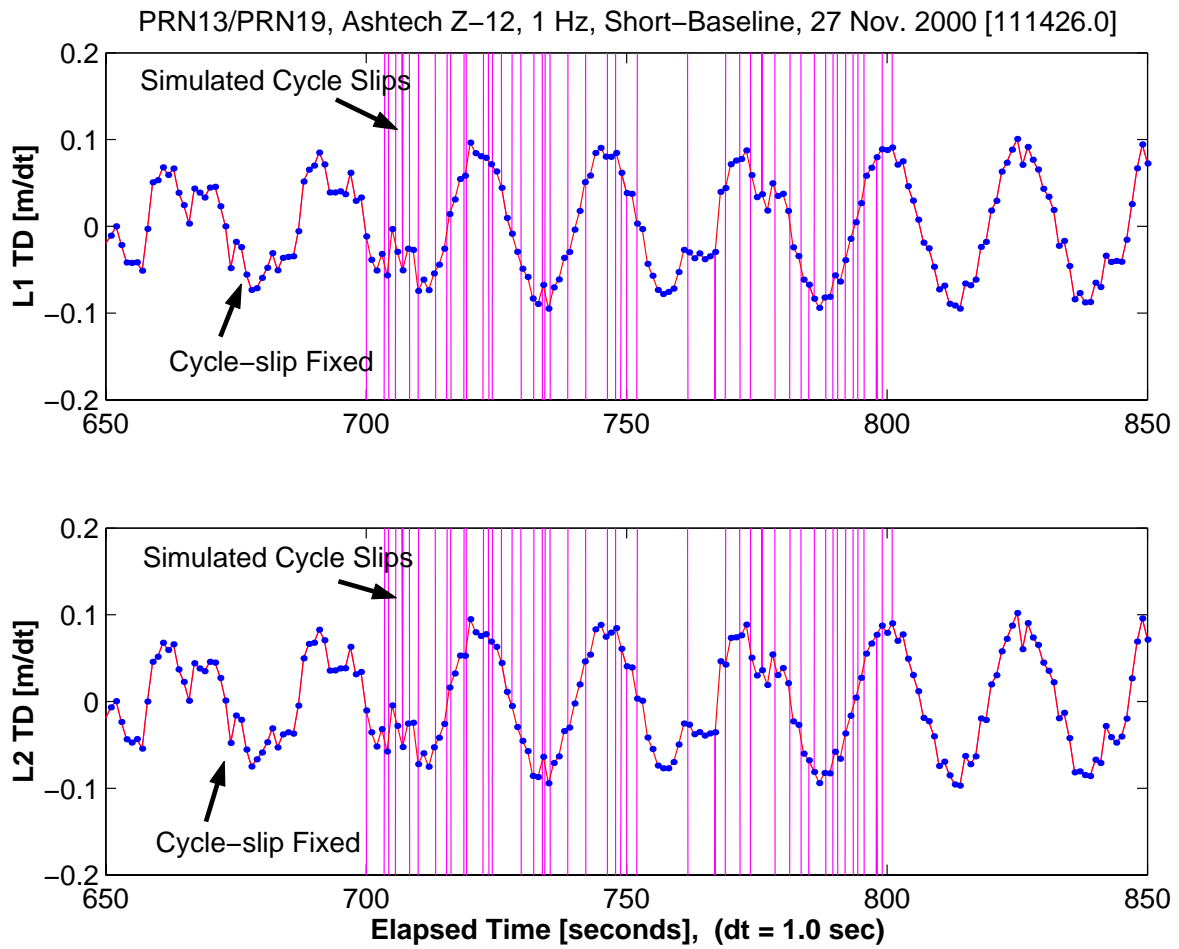


Fig. 16 – Recovery of the simulated cycle slips (Test 4).